Dilution of boundary layer cloud condensation nucleus concentrations by free tropospheric entrainment during marine cold air outbreaks

F. Tornow[1,2], A. S. Ackerman[2], A. M. Fridlind[2], B. Cairns[2], E. C. Crosbie[3,4], S. Kirschler[5,6], R. H. Moore[3], D. Painemal[3,4], C. E. Robinson[3,4], C. Seethala[7], M. A. Shook[3], C. Voigt[5,6], E. L. Winstead[3,4], L. D. Ziemba[3], P. Zuidema[7], A. Sorooshian[8,9]

[1]Earth Institute, Columbia University, NY, 10025, NY
[2]NASA Goddard Institute for Space Studies, NY, 10025, NY
[3]NASA Langley Research Center, Hampton, VA 23681, USA
[4]Science, Systems, and Applications, Inc., Hampton, VA 23681, USA
[5]Deutsches Zentrum für Luft- und Raumfahrt (DLR), Oberpfaffenhofen, Germany
[6]Johannes Gutenberg-Universität, Mainz, Germany
[7]Rosenstiel School of Marine and Atmosphere Science, University of Miami, FL, 33149, USA
[8]Department of Chemical and Environmental Engineering, University of Arizona, Tucson, Arizona, 85721, USA
[9]Department of Hydrology and Atmospheric Sciences, University of Arizona, Tucson, Arizona, 85721, USA

Key Points:

- Recent aircraft measurements enable an analysis of cloud condensation nuclei (CCN) during marine cold air outbreaks.
- CCN concentrations are usually less in the free troposphere than in the marine boundary layer over the northwest Atlantic.
- A boundary layer CCN budget indicates a leading role of entrainment dilution upwind of cloud-regime transition.

Corresponding author: Florian Tornow, `florian.tornow@nasa.gov`

Abstract

Recent aircraft measurements over the northwest Atlantic enable an investigation of how entrainment from the free troposphere (FT) impacts cloud condensation nucleus (CCN) concentrations in the marine boundary layer (MBL) during cold-air outbreaks (CAOs), motivated by the role of CCN in mediating transitions from closed to open-cell regimes. Observations compiled over eight flights indicate predominantly far lesser CCN concentrations in the FT than in the MBL. For one flight, a fetch-dependent MBL-mean CCN budget is compiled from estimates of sea-surface fluxes, entrainment of FT air, and hydrometeor collision-coalescence, based on in-situ and remote-sensing measurements. Results indicate a dominant role of FT entrainment in reducing MBL CCN concentrations, consistent with satellite-observed trends in droplet number concentration upwind of CAO cloud-regime transitions over the northwest Atlantic. Relatively scant CCN may widely be associated with FT dry intrusions, and should accelerate cloud-regime transitions where underlying MBL air is CCN-rich, thereby reducing regional albedo.

Plain Language Summary

Cloud droplets form on a subset of atmospheric particles, referred to as cloud condensation nuclei (CCN). The number concentration of CCN affects the brightness and horizontal extent of clouds. Satellite measurements indicate cloud droplet number concentrations drop off sharply as wintertime marine cold-air outbreak clouds flow eastward, helping to reduce the brightness and horizontal extent of the clouds. We use aircraft measurements from several flights where cold continental air flowing over the northwest Atlantic to estimate the CCN budget in the near-surface turbulent air. We show that CCN concentrations in the immediately overlying air, the free troposphere (FT), are usually far less than in the marine boundary layer (MBL). Through additional analysis of one flight, we show that mixing of FT air is the primary factor reducing CCN concentrations in the MBL prior to rain formation, thereby contributing to a reduction in cloud brightness and extent.

1 Introduction

Extratropical marine boundary layer (MBL) clouds typically occupy the postfrontal sector of synoptic systems when passing over the ocean surface (e.g., Field & Wood, 2007; Rémillard & Tselioudis, 2015). Their presence substantially enhances regional albedo, and such clouds are challenging to faithfully represent in numerical models, whether for forecasting weather or projecting climate change (e.g., Bodas-Salcedo et al., 2016; Forbes & Ahlgrimm, 2014; Tselioudis et al., 2021). Common during winter and its shoulder seasons, cold air outbreaks (CAOs) pose a particular challenge (e.g., Abel et al., 2017; Field et al., 2017) as they form highly reflective, nearly overcast cloud decks, typically organized in roll-like structures that contain both water and ice, which generally break up into less reflective, open-cellular cloud fields farther downwind (e.g., Brümmer, 1999; Pithan et al., 2019).

MBL clouds are sensitive to the number concentration of aerosol available as cloud condensation nuclei (CCN). Greater CCN concentrations can enhance cloud albedo when (1) distributing the same cloud condensate over more numerous, smaller droplets (Twomey, 1974), (2) suppressing precipitation formation, leading to greater areal cloud cover (Albrecht, 1989) and thicker clouds (Pincus & Baker, 1994), and (3) affecting cloud mesoscale structure (e.g., H. Wang & Feingold, 2009). On the other hand, smaller droplets fall more slowly in updrafts and can boost entrainment of overlying dry air, reducing cloud thickness and counteracting albedo-enhancing effects (Ackerman et al., 2004; Bretherton et al., 2007). The collisions between hydrometeors that drive precipitation formation in warm clouds also reduce CCN number concentrations and can drive a positive feedback loop in which fewer CCN promote further precipitation formation in warm stratocumulus (Yamaguchi

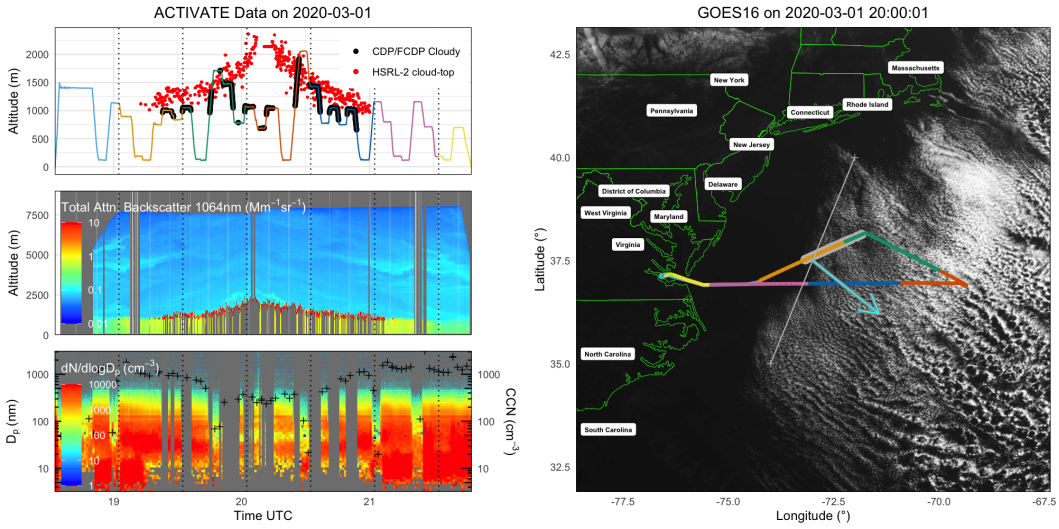

Figure 1. ACTIVATE Falcon flight track during RF14 on 1 March 2020 (top left and right), King-Air HSRL-2 remote-sensing measurements (top and middle left), Falcon in-situ measurements of aerosol PSD and CCN concentrations at 0.43 % supersaturation (bottom left), and GOES-16 visible image (right) with approximate wind direction inferred from roll orientation (cyan line), cloud edge (white line), and King-Air RSP measurement extent (gray on either side of the flight track).

et al., 2017). Such a feedback loop is also implicated in mixed-phase CAO observations (e.g., Abel et al., 2017) and simulations (Tornow et al., 2021), and is hypothesized to explain horizontal gradients in cloud droplet number concentrations off the mid-Atlantic coast of the US (Dadashazar et al., 2021).

Unique to CAOs are extreme surface heat fluxes aided by the warm temperatures of the Gulf Stream (Liu et al., 2014; Seethala et al., 2021) that typically drive rapid MBL deepening despite strong large-scale subsidence (Papritz et al., 2015; Papritz & Spengler, 2017), thereby copiously entraining free tropospheric (FT) air. The MBL air, because it advects off of the industrialized, urban eastern US seaboard, can be highly polluted (Sorooshian et al., 2020), setting up a large potential influence for the FT air. Other sinks and sources in each airmass may include new particle formation (e.g., I. L. McCoy et al., 2021; Zheng et al., 2021) and long-range transport of direct emissions, such as biomass burning (e.g., Zheng et al., 2020).

In previous work, simulated MBL clouds in a northwest Atlantic CAO case study were found sensitive to idealized FT–MBL differences in CCN concentration (Tornow et al., 2021). Here we use observations of CAOs in that region to assess actual FT-MBL CCN differences and the role that entrainment of FT air plays in the MBL CCN budget as it evolves downwind. This wider analysis is enabled by recent in-situ and remote-sensing observations collected on multiple research flights during the Aerosol Cloud Meteorology Interactions over the Western Atlantic Experiment (ACTIVATE; Sorooshian et al., 2019).). In the following we first present evidence from multiple flights that the FT predominantly dilutes MBL CCN before heavy precipitation develops. We then quantify the MBL CCN budget for one case study, revealing the dominant role of FT dilution on MBL CCN evolution upwind of heavy precipitation.

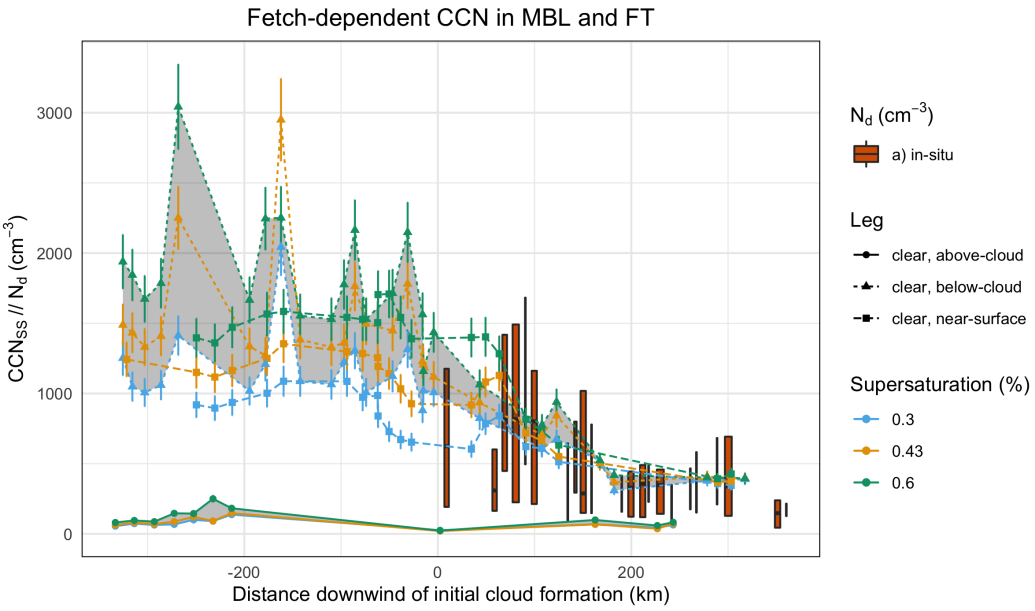

Figure 2. CCN at selected supersaturations (by color) in cloud-free legs on RF14 versus downwind distance, ΔL, derived via a projection of leg geolocation from cloud edge in the direction of the large-scale horizontal wind (shown in Figure 1). Leg types distinguished per legend. Gray shading spans FT class "clear, above-cloud" and MBL class "clear, below-cloud". Red bars span middle half of in-cloud droplet concentration N_d from FCDP, with median indicated.

2 CCN gap between FT and MBL

Before surveying the measurements across several flights, we first provide a composite demonstration of in-situ and remote sensing data gathered during one research flight (RF14) in Figure 1. In-situ legs are classified by their cloud-relative vertical position and projected into a quasi-Lagrangian framework (methods in Section S1). The processed CCN measurements for RF14 seen in Figure 2 demonstrate the analysis approach subsequently applied to all flights. The differences between "clear, near-surface" and "clear, below-cloud" samples are smaller than the variability within each group, consistent with relatively well-mixed conditions within a turbulent MBL. Upwind of the cloud edge, entrainment of FT air can only reduce the MBL CCN, since the FT concentrations (at SS = 0.3-0.6%) are relatively stable at 50-200 cm^{-3}, much less than MBL concentrations of 1000-3000 cm^{-3}. The CCN gap between FT and MBL progressively narrows as MBL concentrations decrease downwind of the cloud edge, consistent with dilution via strong FT entrainment . At all downwind distances sampled during this flight, FT concentrations are well exceeded by those in the MBL.

Another prominent feature in Figure 2 is a decrease in CCN spectral width downwind: upwind of cloud formation ($\Delta L \approx$ -300 km) nearly twice the particles are available for activation as SS increases from 0.3 to 0.6%, whereas downwind ($\Delta L \approx$ 200 km) only ∼20% more particles are available when doubling SS.

To assess whether the FT commonly dilutes MBL CCN in northwest Atlantic CAOs, we compare MBL and FT $CCN_{SS=0.43\%}$ (hereafter just "CCN") concentrations versus ΔL in Figure 3a. FT concentrations are predominantly exceeded by those in the MBL with rare exceptions. Some instances, such as those corresponding to RF17 and RF18, may be associated with crosswind flight paths subject to variability in upwind conditions (Figure S8). Owing to the northerly winds that day, air sampled farther offshore traveled longer over the ocean prior to cloud formation, and the indication in Figure 3 that

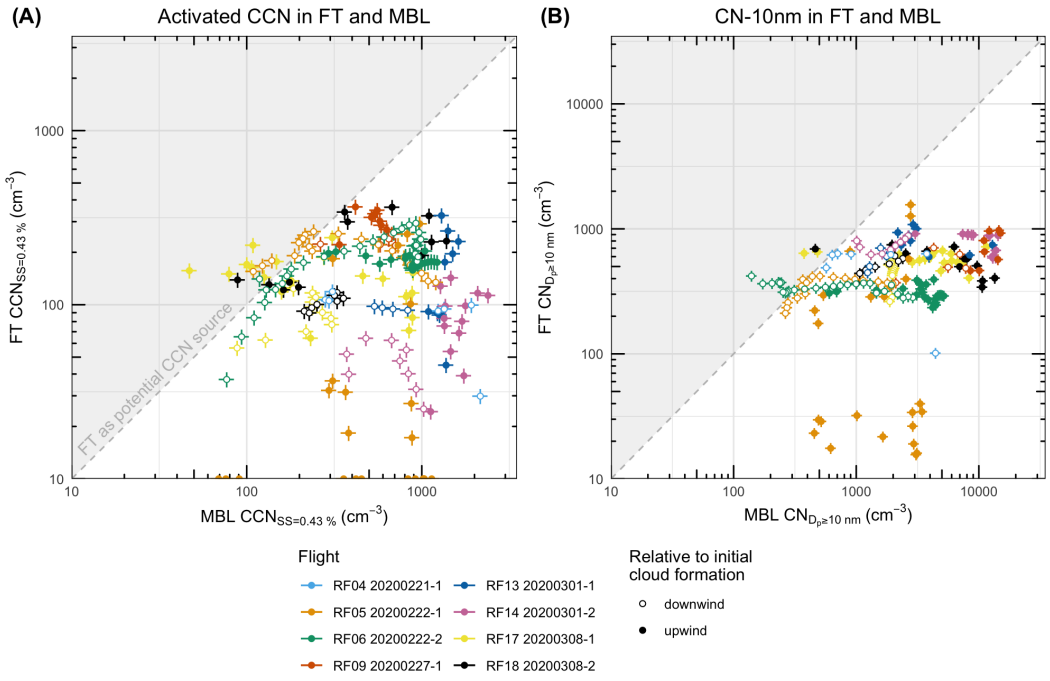

Figure 3. FT versus MBL concentration of CCN at 0.43% supersaturation (left) and of CN greater than or equal to 10 nm diameter (right) colored by research flight (per legend) and interpolated at 25-km intervals across available ΔL. Filled and open circles show the relative position up- and downwind, respectively, to the cloud edge.

the FT served briefly as a CCN source from both flights that day may be attributable to spatiotemporal variability neglected in our approach.

Because supersaturations in CAO convection can be expected to exceed 0.43%, we also evaluate how particles activating at greater supersaturations affect the FT–MBL differences. For condendation nuclei (CN) larger than or equal to 10 nm, which include sizes far smaller than are likely activated in MBL clouds, qualitatively similar gaps are seen in Figure 3b.

We also find that the FT–MBL CCN gap generally narrows downwind of cloud formation because of decreasing MBL concentrations (open symbols tend to lie to the left of closed symbols), consistent with RF14 (Figure 2). Meanwhile, FT concentrations generally lack systematic trends with downwind distance and are characterized by a much smaller absolute dynamic range (cf. Figure 2).

In summary, in-situ observations collected over several CAO events consistently indicate a predominance of CCN-poor conditions in the FT and a CCN gap between FT and MBL that progressively narrows downwind.

3 Impact of FT entrainment on MBL CCN

In Section 2 we aggregated transits across the MBL top to assess FT-MBL CCN differences for several flights. Since RF14 is a particularly long flight with multiple transits, we can further estimate for that flight the relative contribution of FT entrainment to MBL CCN evolution downwind. To do so, we estimate budget terms based on in-situ and remote sensing observations (Section 3.1) and evaluate their evolution with fetch (Section 3.2).

3.1 CCN budget terms

3.1.1 Entrainment

The MBL entrainment rate is notoriously challenging to quantify, so much that its determination was a primary objective of a field campaign targeting subtropical stratocumulus (e.g., Stevens et al., 2003; Faloona et al., 2005). As will be seen below, the entrainment term not only dominates the MBL CCN budget upwind of strong precipitation, but the magnitude of its uncertainty is also much greater than that for other budget terms. We address that uncertainty here by deriving two independent estimates of entrainment rate and its dependence on downwind fetch. As a primary method that is used in the CCN budget, we exploit the fetch-dependent difference between CO trace gas measured in the FT and MBL to estimate entrainment rates by using a mixed-layer approach (e.g., Lilly, 1968; Fridlind et al., 2012) that we apply to a horizontally translating quasi-Lagrangian MBL. As a second method for comparison with the CO-derived entrainment rates, we combine retrievals of cloud-top height from Geostationary Operational Environmental Satellites GOES-16 observations (Minnis et al., 2008), constituting a Lagrangian counterpart to the analysis by Painemal et al. (2017), with subsidence rates from reanalysis (European Center for Medium Range Weather Forecast Reanalysis 5$^{\text{th}}$ Generation, ERA5; Hersbach et al., 2020) along Lagrangian trajectories computed from ERA5 horizontal winds.

To compute the actual entrainment term for the MBL CCN budget, we multiply the CO-derived entrainment rate by the corresponding measured FT–MBL difference in $\text{CCN}_{\text{SS=0.43\%}}$. The details of our entrainment calculations are described further in Section S1.3.1.

3.1.2 Hydrometeor collisions

We approximate loss of (activated) CCN from hydrometeor collision through a combination of more continuous remote sensing measurements and more detailed in-situ measurements. More specifically, we use hydrometeor particle size distributions (PSDs) measured in-situ to stochastically reconstruct PSD profiles within the cloudy MBL that vary with fetch owing to the progressive deepening of the MBL depth and corresponding increase in LWP, as well decreasing droplet concentration N_d in response to a progressively increasing rate of hydrometeor collisions. Loss rates are computed using a simplified stochastic collection equation (cf. Wood, 2006), which we simply treat as the loss rate for CCN. To fill in gaps in our fetch-dependent CCN budget, we use LWP retrievals from the Research Scanning Polarimeter (RSP) to constrain our reconstruction profiles, which are available at $0 < \Delta L < 100$ km (shaded gray in Figure 4), well upwind of the cloud transition seen in Figure 1. To extend our budget further downwind than afforded by RSP retrievals, we also use retrievals from the satellite-borne Moderate Resolution Imaging Spectroradiometer (MODIS) on the Aqua satellite acquired 1 hour before the flight to extend our approximation. The details of our collisional loss calculations are described further in Section S1.3.2.

3.1.3 Surface source

We estimate a MBL-mean sea-salt surface source following Wood et al. (2017), as originally formulated by Clarke et al. (2006): $\dot{N}_{\text{surf}} = \frac{F u_s^{3.41}}{H}$, in which $F = 132$ m^{-3} (m s^{-1})$^{-2.41}$, near-surface wind speed u_s is taken from the ERA5 winds, and H from a polynomial fit to cloud-top height as measured by the High Spectral Resolution Lidar HSRL-2, as described further in Section S1.3.1.

3.2 Budget results

FT entrainment rates based on CO measurements in the MBL and FT (Figure S2) are substantial, reaching up to 12 cm s^{-1} for $0 < \Delta L < 100$ km (Figure 4a). These CO-based estimates overlap remarkably well with our independent estimates obtained from GOES-16 retrievals in combination with ERA5 winds. These entrainment rates are also comparable to those from large-eddy simulation of a CAO in the same region and season, which reach peak rate of 10 cm s^{-1} just before the rain onset (cf. Figure 2 of Tornow et al., 2021).

Entrainment rate estimates along Lagrangian trajectories intersecting the flight track that were repeated hourly reveal substantial variability across the range of fetch (Fig. S3c). Whether using measurements obtained from a platform moving much faster than the MBL, with the aircraft speed of ∼100 m s^{-1} and horizontal winds in the MBL of ∼25 m s^{-1}, or using instantaneous measurements (e.g., from MODIS on a polar-orbiting satellite), we inherently assume stationary conditions, a simplifying assumption that can introduce substantial uncertainties in our semi-Lagrangian framework. Nonetheless, entrainment rates derived from our best estimate of a true Lagrangian framework are comparable with those computed from the same inputs in our quasi-Lagrangian framework for RF14, as seen in Figure S3c. Thus we expect that the quasi-Lagrangian transformation is generally sufficient to provide a plausible dependence of fetch-dependent dilution of MBL CCN by FT entrainment across the collection of flights, consistent with our interpretation of Figures 2 and 3.

Results in Figure 4b indicate that the observed evolution in MBL CCN concentration (∼ -240 cm^{-3} h^{-1}) is primarily explained by FT entrainment (∼ -180 cm^{-3} h^{-1}), while hydrometeor collisions are less important (∼ -25 cm^{-3} h^{-1}) and surface production is quite modest (∼5 cm^{-3} h^{-1}). These relative contributions to the CCN budget are consistent with the aforementioned northwest Atlantic CAO simulations that used idealized aerosol in the absence of in-situ measurements (cf. Figure 6 of Tornow et al., 2021). Constraining the PSD profiles with collisional loss rates with MODIS retrievals of LWP (dashed lines in Figure 4), a growing role for hydrometeor collisions is indicated approaching the cloud-regime transition, resulting from the presence of larger drops as well as frozen hydrometeors (riming), which start to dominate the CCN budget at $\Delta L >$ 200 km.

4 Discussion

It is unsurprising that such substantial entrainment rates occur in the early stage of marine CAOs, an environment where the MBL can deepen rapidly owing to enormous surface fluxes, despite large-scale subsidence (e.g., Fig. S3b); aside, we note both MBL deepening and subsidence contribute to entrainment. What is surprising is the consistently large FT-MBL gaps in CCN concentrations, which facilitate strong CCN dilution of the MBL from entrainment.

An obvious question arises: where did such relatively clean FT air originate? Seven-day back-trajectories arriving at 2 and 3 km altitude for RF14 (Figure S9) indicate a northwest origin, respectively starting near Alaska and the north Pacific and reaching ∼6 km altitude before subsiding. Such a pattern matches the flow of FT dry intrusions (e.g., Jaeglé et al., 2017; Raveh-Rubin, 2017) that frequently descend into the postfrontal sector of extratropical cyclones downwind of the US east coast where CCN-rich boundary layer air moves offshore. Remote regions, such as the Southern Ocean, also experience FT dry intrusions (Raveh-Rubin, 2017) but there it is unclear whether the FT is comparably CCN-poor relative to the MBL; we note that Antarctic air during winter has few aerosol sources compared to the open ocean (Papritz et al., 2015). For an MBL that is CCN-poor, from a lack of aerosol sources within the (continental) boundary layer upwind, or for overlying FT air that is CCN-rich, whether from advected pollutants (e.g., Zheng et al., 2020) or aerosol nucleation (cf. I. L. McCoy et al., 2021, though least likely

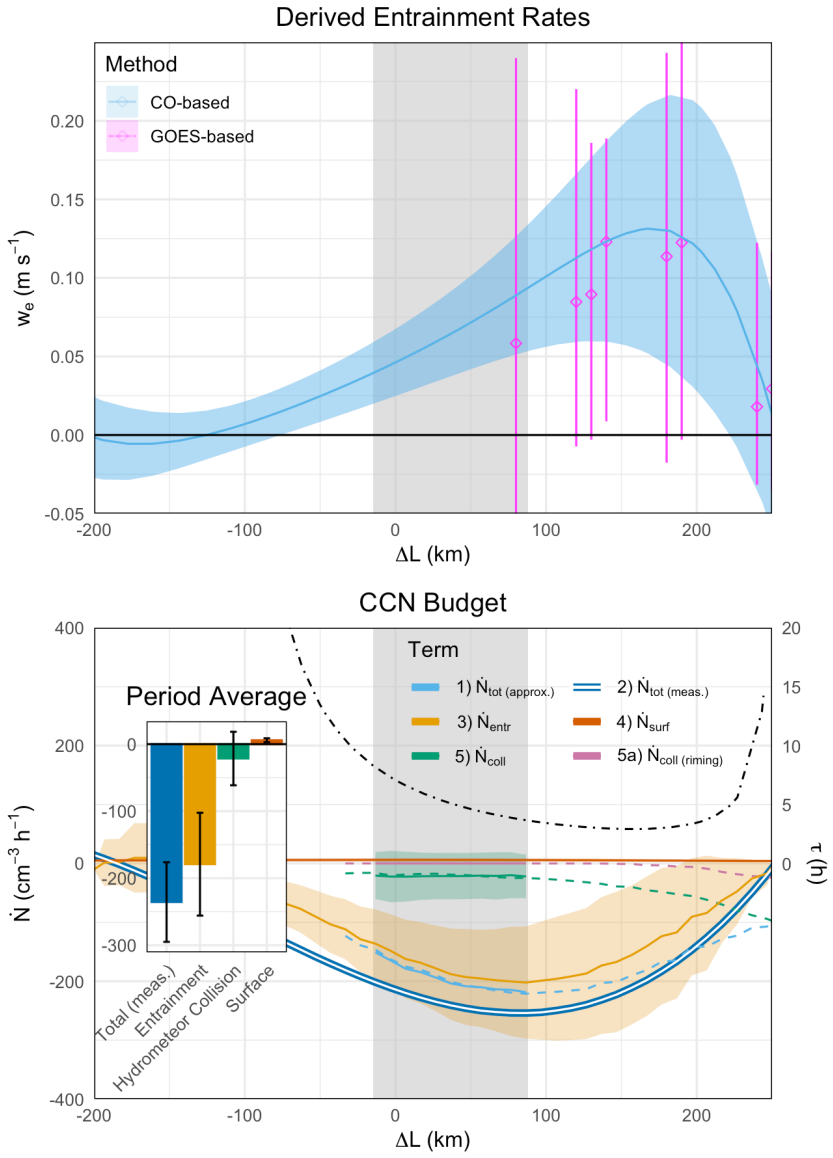

Figure 4. Estimated entrainment rates (top) and quasi-Lagrangian MBL CCN budget terms (bottom) versus ΔL (as in Figure 2) for RF14. Entrainment rates were derived from a mixed-layer framework (blue) with shaded uncertainties (+/- one standard error) and from geostationary CTH retrievals along ERA5 trajectories (magenta) where intersecting the flight track (see also Fig. S3 for more details); Symbols in the top panel indicate median values and error bars span 5$^{\text{th}}$ to 95$^{\text{th}}$ percentiles of entrainment rates that we obtain from an array of trajectories, as described in Section S1.3.1. Gray shading indicates distance range of budget analysis using RSP. Budget terms include FT entrainment (orange), hydrometeor collisions (green) and contribution of riming (pink), surface source (red), their sum (light blue), and measured change of $\text{CCN}_{\text{SS=0.43\%}}$ (dark blue with white stripe). For entrainment, surface, and collision terms, uncertainties are shown (+/- one standard error). Collision rates using MODIS LWP retrievals (dashed lines) extend those from RSP. Inset: budget terms averaged over shaded area with uncertainties (+/- one standard error). The black, dot-dashed line shows characteristic entrainment timescale, computed as $\tau = H/w_e$ per Diamond et al. (2018)

in winter months), CCN concentrations in the FT could approach or exceed those in the MBL, weakening MBL dilution or even buffering microphysically induced reductions in MBL CCN concentrations.

Our analysis points to CCN dilution via FT entrainment as a plausible leading explanation for satellite-observed N_d gradients close to the US East Coast during winter (Painemal et al., 2021). Such N_d gradients are particularly strong during CAOs (Dadashazar et al., 2021), coincident with greater than usual growth in cloud-top height. Dadashazar et al. (2021) furthermore suggest a similar FT–MBL CCN difference from aerosol extinction retrievals. Our findings are also consistent with CAO simulations (Tornow et al., 2021), which yield comparable entrainment rates and relative roles of FT entrainment and hydrometeor collisional loss upwind of intense precipitation. A characteristic timescale H/w_e at which entrainment equilibrates the MBL with the FT is ∼3 h for much of the fetch (Figure 4b), an order of magnitude faster than in subtropical stratocumulus (Diamond et al., 2018), highlighting the rapidity at which the MBL is mixed with FT air upwind of strong precipitation in CAOs. Once downwind of precipitation (i.e., farther offshore than reached in RF14), entrainment typically declines, associated with a plateauing and then declining MBL depth. At this later stage, MBL CCN concentrations are found to approach or even be exceeded by (relatively steady) FT concentrations, as observed near Graciosa Island (Tomlin et al., 2021), mainly caused by rapid CCN loss during formation of intense precipitation within the MBL as indicated by previous CAO observations (Abel et al., 2017) and simulations (Tornow et al., 2021), allowing the FT to act as CCN buffer to the MBL (Wood et al., 2017).

The MBL CCN budget analysis is subject to some potential weaknesses beyond those already described. First, we use CCN at a fixed SS = 0.43%, whereas collisional loss applies to aerosol particles activated over a range of supersaturations. Second, the ERA5 reanalysis is known to overestimate zonal winds in the region but values are expected to be within 10% (Belmonte Rivas & Stoffelen, 2019; Seethala et al., 2021). Third, we neglect chemical sources of CCN at any given SS, such as new particle formation (although MBL total aerosol surface areas are unfavorable) and aqueous-phase processes that allow dissolved aerosol particles to activate at lower SS in subsequent cloud cycles (e.g., Y. Wang et al., 2021). Fourth, a chain of assumptions is required to construct MBL cloud profiles for collision-coalescence calculations. The sizable error bars in Figure 4 are intended to encapsulate these uncertainties.

Finally, CCN dilution from FT entrainment should serve to accelerate precipitation formation and the associated transition towards broken cloud fields of cellular convection. Compared to transition-accelerating CCN loss from riming (e.g., Tornow et al., 2021), which is highly uncertain owing in large part to poorly-known ice formation pathways (Korolev et al., 2020; Korolev & Leisner, 2020), our analysis indicates CCN dilution to be common in CAOs downwind of non-pristine regions and upwind of intense precipitation. Cloud-climate feedbacks in Earth system model results may be sensitive to precipitation formation in such CAOs (D. T. McCoy et al., 2020), indicating a need to capture such aerosol entrainment regionally in order to faithfully simulate cloud regime transitions.

5 Conclusions

A quasi-Lagrangian analysis of recent measurements collected from eight aircraft flights under cold-air outbreak (CAO) conditions during the ACTIVATE field campaign supports the following conclusions:

- Cloud condensation nucleus (CCN) concentrations in the marine boundary layer (MBL) at supersaturations of 0.3 to 0.6%, as well as condensation nuclei larger than 10 nm, are predominantly far greater than in the free troposphere (FT) upwind of intense precipitation in CAOs over the northwest Atlantic.

- Based on the research flight that reached farthest downwind, a budget analysis of CCN concentration in the MBL computed from available in-situ and remote-sensing measurements identifies MBL dilution from rapid entrainment of FT air as the primary sink of CCN upwind of cloud-regime transitions.
- The budget analysis indicates a characteristic timescale at which entrainment equilibrates the MBL aerosol with the FT aerosol of ∼3 hours, which is roughly an order of magnitude faster than found in subtropical stratocumulus owing to rapid MBL deepening under strong subsidence in CAOs.
- CCN dilution from FT entrainment should accelerate precipitation formation and cloud closed-to-open cell transitions, reducing regional albedo in CAOs fed by similar FT air masses that are often associated with dry intrusions.

Open Research

All data is available at `https://www-air.larc.nasa.gov/cgi-bin/ArcView/activate.2019`. The R code written to evaluate data is available upon request.

Acknowledgments

This work was supported by ACTIVATE, a NASA Earth Venture Suborbital-3 (EVS-3) investigation funded by NASA's Earth Science Division and managed through the Earth System Science Pathfinder Program Office Division (grant no. 80NSSC19K044). We thank the ACTIVATE team for helpful discussion and for support with measurements and quality control. C.V. and S.K. thank funding by the Deutsche Forschungsgemeinschaft (DFG, German Research Foundation) – TRR 301 – Project-ID 428312742 and SPP 1294 HALO under contract VO 1504/7-1. A.S.A and A.M.F. were supported by the NASA Modeling, Analysis and Prediction Program. We thank two anonymous reviewers for their helpful comments that improved this work.

References

Abel, S. J., Boutle, I. A., Waite, K., Fox, S., Brown, P. R. A., Cotton, R., ... Bower, K. N. (2017). The role of precipitation in controlling the transition from stratocumulus to cumulus clouds in a northern hemisphere cold-air outbreak. *Journal of the Atmospheric Sciences*, *74*(7), 2293 - 2314. Retrieved from `https://journals.ametsoc.org/view/journals/atsc/74/7/jas-d-16-0362.1.xml` doi: 10.1175/JAS-D-16-0362.1

Ackerman, A. S., Kirkpatrick, M., & Stevens, D. (2004). The impact of humidity above stratiform clouds on indirect aerosol climate forcing. *Nature*, *432*, 1014–1017. Retrieved from `https://www.nature.com/articles/nature03174` doi: 10.1038/nature03174

Albrecht, B. A. (1989). Aerosols, cloud microphysics, and fractional cloudiness. *Science*, *245*(4923), 1227-1230. Retrieved from `https://www.science.org/doi/10.1126/science.245.4923.1227` doi: 10.1126/science.245.4923.1227

Belmonte Rivas, M., & Stoffelen, A. (2019). Characterizing era-interim and era5 surface wind biases using ascat. *Ocean Science*, *15*(3), 831–852. Retrieved from `https://os.copernicus.org/articles/15/831/2019/` doi: 10.5194/os-15-831-2019

Bodas-Salcedo, A., Hill, P. G., Furtado, K., Williams, K. D., Field, P. R., Manners, J. C., ... Kato, S. (2016). Large contribution of supercooled liquid clouds to the solar radiation budget of the southern ocean. *Journal of Climate*, *29*(11), 4213 - 4228. Retrieved from `https://journals.ametsoc.org/view/journals/clim/29/11/jcli-d-15-0564.1.xml` doi: 10.1175/JCLI-D-15-0564.1

Bretherton, C. S., Blossey, P. N., & Uchida, J. (2007). Cloud droplet sedimenta-

tion, entrainment efficiency, and subtropical stratocumulus albedo. *Geophysical Research Letters*, *34*(3). Retrieved from https://agupubs.onlinelibrary.wiley.com/doi/abs/10.1029/2006GL027648 doi: https://doi.org/10.1029/2006GL027648

Brümmer, B. (1999). Roll and cell convection in wintertime arctic cold-air outbreaks. *Journal of the Atmospheric Sciences*, *56*(15), 2613 - 2636. Retrieved from https://journals.ametsoc.org/view/journals/atsc/56/15/1520-0469_1999_056_2613_racciw_2.0.co_2.xml doi: 10.1175/1520-0469(1999)056⟨2613:RACCIW⟩2.0.CO;2

Clarke, A. D., Owens, S. R., & Zhou, J. (2006). An ultrafine sea-salt flux from breaking waves: Implications for cloud condensation nuclei in the remote marine atmosphere. *Journal of Geophysical Research: Atmospheres*, *111*(D6). Retrieved from https://agupubs.onlinelibrary.wiley.com/doi/abs/10.1029/2005JD006565 doi: 10.1029/2005JD006565

Dadashazar, H., Painemal, D., Alipanah, M., Brunke, M., Chellappan, S., Corral, A. F., ... Sorooshian, A. (2021). Cloud drop number concentrations over the western north atlantic ocean: seasonal cycle, aerosol interrelationships, and other influential factors. *Atmospheric Chemistry and Physics*, *21*(13), 10499–10526. Retrieved from https://acp.copernicus.org/articles/21/10499/2021/ doi: 10.5194/acp-21-10499-2021

Diamond, M. S., Dobracki, A., Freitag, S., Small Griswold, J. D., Heikkila, A., Howell, S. G., ... Wood, R. (2018). Time-dependent entrainment of smoke presents an observational challenge for assessing aerosol–cloud interactions over the southeast atlantic ocean. *Atmospheric Chemistry and Physics*, *18*(19), 14623–14636. Retrieved from https://acp.copernicus.org/articles/18/14623/2018/ doi: 10.5194/acp-18-14623-2018

Faloona, I., Lenschow, D. H., Campos, T., Stevens, B., van Zanten, M., Blomquist, B., ... Gerber, H. (2005). Observations of entrainment in eastern pacific marine stratocumulus using three conserved scalars. *Journal of the Atmospheric Sciences*, *62*(9), 3268 - 3285. Retrieved from https://journals.ametsoc.org/view/journals/atsc/62/9/jas3541.1.xml doi: 10.1175/JAS3541.1

Field, P. R., Brozkova, R., Chen, M., Dudhia, J., Lac, C., Hara, T., ... McTaggart-Cowan, R. (2017). Exploring the convective grey zone with regional simulations of a cold air outbreak. *Quarterly Journal of the Royal Meteorological Society*, *143*(707), 2537-2555. Retrieved from https://rmets.onlinelibrary.wiley.com/doi/full/10.1002/qj.3105 doi: https://doi.org/10.1002/qj.3105

Field, P. R., & Wood, R. (2007). Precipitation and cloud structure in midlatitude cyclones. *Journal of Climate*, *20*(2), 233 - 254. Retrieved from https://journals.ametsoc.org/view/journals/clim/20/2/jcli3998.1.xml doi: 10.1175/JCLI3998.1

Forbes, R. M., & Ahlgrimm, M. (2014). On the representation of high-latitude boundary layer mixed-phase cloud in the ecmwf global model. *Monthly Weather Review*, *142*(9), 3425 - 3445. Retrieved from https://journals.ametsoc.org/view/journals/mwre/142/9/mwr-d-13-00325.1.xml doi: 10.1175/MWR-D-13-00325.1

Fridlind, A. M., Ackerman, A. S., Chaboureau, J.-P., Fan, J., Grabowski, W. W., Hill, A. A., ... Zhang, M. (2012). A comparison of twp-ice observational data with cloud-resolving model results. *Journal of Geophysical Research: Atmospheres*, *117*(D5). Retrieved from https://agupubs.onlinelibrary.wiley.com/doi/abs/10.1029/2011JD016595 doi: 10.1029/2011JD016595

Hersbach, H., Bell, B., Berrisford, P., Hirahara, S., Horányi, A., Muñoz-Sabater, J., ... Thépaut, J.-N. (2020). The era5 global reanalysis. *Quarterly Journal of the Royal Meteorological Society*, *146*(730), 1999-2049. Retrieved from

https://rmets.onlinelibrary.wiley.com/doi/abs/10.1002/qj.3803 doi: https://doi.org/10.1002/qj.3803

Jaeglé, L., Wood, R., & Wargan, K. (2017). Multiyear composite view of ozone enhancements and stratosphere-to-troposphere transport in dry intrusions of northern hemisphere extratropical cyclones. *Journal of Geophysical Research: Atmospheres*, *122*(24), 13,436-13,457. Retrieved from https://agupubs.onlinelibrary.wiley.com/doi/abs/10.1002/2017JD027656 doi: https://doi.org/10.1002/2017JD027656

Korolev, A., Heckman, I., Wolde, M., Ackerman, A. S., Fridlind, A. M., Ladino, L. A., ... Williams, E. (2020). A new look at the environmental conditions favorable to secondary ice production. *Atmospheric Chemistry and Physics*, *20*(3), 1391–1429. Retrieved from https://acp.copernicus.org/articles/20/1391/2020/ doi: 10.5194/acp-20-1391-2020

Korolev, A., & Leisner, T. (2020). Review of experimental studies of secondary ice production. *Atmospheric Chemistry and Physics*, *20*(20), 11767–11797. Retrieved from https://acp.copernicus.org/articles/20/11767/2020/ doi: 10.5194/acp-20-11767-2020

Li, X.-Y., Wang, H., Chen, J., Endo, S., George, G., Cairns, B., ... Zuidema, P. (2021). Large-eddy simulations of marine boundary-layer clouds associated with cold air outbreaks during the activate campaign– part 1: Case setup and sensitivities to large-scale forcings. *Journal of the Atmospheric Sciences*. Retrieved from https://journals.ametsoc.org/view/journals/atsc/aop/JAS-D-21-0123.1/JAS-D-21-0123.1.xml doi: 10.1175/JAS-D-21-0123.1

Lilly, D. K. (1968). Models of cloud-topped mixed layers under a strong inversion. *Quarterly Journal of the Royal Meteorological Society*, *94*(401), 292-309. Retrieved from https://rmets.onlinelibrary.wiley.com/doi/abs/10.1002/qj.49709440106 doi: https://doi.org/10.1002/qj.49709440106

Liu, J.-W., Xie, S.-P., Norris, J. R., & Zhang, S.-P. (2014). Low-level cloud response to the gulf stream front in winter using calipso. *Journal of Climate*, *27*(12), 4421 - 4432. Retrieved from https://journals.ametsoc.org/view/journals/clim/27/12/jcli-d-13-00469.1.xml doi: 10.1175/JCLI-D-13-00469.1

McCoy, D. T., Field, P., Bodas-Salcedo, A., Elsaesser, G. S., & Zelinka, M. D. (2020). A regime-oriented approach to observationally constraining extratropical shortwave cloud feedbacks. *Journal of Climate*, *33*(23), 9967 - 9983. Retrieved from https://journals.ametsoc.org/view/journals/clim/33/23/jcliD190987.xml doi: 10.1175/JCLI-D-19-0987.1

McCoy, I. L., Bretherton, C. S., Wood, R., Twohy, C. H., Gettelman, A., Bardeen, C. G., & Toohey, D. W. (2021). Influences of recent particle formation on southern ocean aerosol variability and low cloud properties. *Journal of Geophysical Research: Atmospheres*, *126*(8), e2020JD033529. Retrieved from https://agupubs.onlinelibrary.wiley.com/doi/abs/10.1029/2020JD033529 doi: https://doi.org/10.1029/2020JD033529

Minnis, P., Nguyen, L., Palikonda, R., Heck, P. W., Spangenberg, D. A., Doelling, D. R., ... Szedung, S.-M. (2008). Near-real time cloud retrievals from operational and research meteorological satellites. In R. H. Picard, A. Comeron, K. Schäfer, A. Amodeo, & M. van Weele (Eds.), *Remote sensing of clouds and the atmosphere xiii* (Vol. 7107, pp. 19 – 26). SPIE. Retrieved from https://doi.org/10.1117/12.800344 doi: 10.1117/12.800344

Painemal, D., Corral, A. F., Sorooshian, A., Brunke, M. A., Chellappan, S., Afzali Gorooh, V., ... Zuidema, P. (2021). An overview of atmospheric features over the western north atlantic ocean and north american east coast—part 2: Circulation, boundary layer, and clouds. *Journal of Geophysical Research: Atmospheres*, *126*(6), e2020JD033423. Retrieved from https://agupubs.onlinelibrary.wiley.com/doi/abs/10.1029/2020JD033423 doi:

https://doi.org/10.1029/2020JD033423

Painemal, D., Xu, K.-M., Palikonda, R., & Minnis, P. (2017). Entrainment rate diurnal cycle in marine stratiform clouds estimated from geostationary satellite retrievals and a meteorological forecast model. *Geophysical Research Letters*, *44*(14), 7482-7489. Retrieved from https://agupubs.onlinelibrary.wiley.com/doi/abs/10.1002/2017GL074481 doi: https://doi.org/10.1002/2017GL074481

Papritz, L., Pfahl, S., Sodemann, H., & Wernli, H. (2015). A climatology of cold air outbreaks and their impact on air–sea heat fluxes in the high-latitude south pacific. *Journal of Climate*, *28*(1), 342 - 364. Retrieved from https://journals.ametsoc.org/view/journals/clim/28/1/jcli-d-14-00482.1.xml doi: 10.1175/JCLI-D-14-00482.1

Papritz, L., & Spengler, T. (2017). A lagrangian climatology of wintertime cold air outbreaks in the irminger and nordic seas and their role in shaping air–sea heat fluxes. *Journal of Climate*, *30*(8), 2717 - 2737. Retrieved from https://journals.ametsoc.org/view/journals/clim/30/8/jcli-d-16-0605.1.xml doi: 10.1175/JCLI-D-16-0605.1

Pincus, R., & Baker, M. B. (1994). Effect of precipitation on the albedo susceptibility of clouds in the marine boundary layer. *Nature*, *372*(6503), 250 - 252. Retrieved from https://www.nature.com/articles/372250a0 doi: 10.1038/372250a0

Pithan, F., Svensson, G., Caballero, R., Chechin, D., Cronin, T. W., Ekman, A. M. L., ... Wendisch, M. (2019). Role of air-mass transformations in exchange between the arctic and mid-latitudes. *Nature Geoscience*, *11*, 805–812. Retrieved from https://www.nature.com/articles/s41561-018-0234-1 doi: 10.1038/s41561-018-0234-1

Raveh-Rubin, S. (2017). Dry intrusions: Lagrangian climatology and dynamical impact on the planetary boundary layer. *Journal of Climate*, *30*(17), 6661 - 6682. Retrieved from https://journals.ametsoc.org/view/journals/clim/30/17/jcli-d-16-0782.1.xml doi: 10.1175/JCLI-D-16-0782.1

Rémillard, J., & Tselioudis, G. (2015). Cloud regime variability over the azores and its application to climate model evaluation. *Journal of Climate*, *28*(24), 9707 - 9720. Retrieved from https://journals.ametsoc.org/view/journals/clim/28/24/jcli-d-15-0066.1.xml doi: 10.1175/JCLI-D-15-0066.1

Seethala, C., Zuidema, P., Edson, J., Brunke, M., Chen, G., Li, X.-Y., ... Ziemba, L. (2021). On assessing era5 and merra2 representations of cold-air outbreaks across the gulf stream. *Geophysical Research Letters*, *48*(19), e2021GL094364. Retrieved from https://agupubs.onlinelibrary.wiley.com/doi/abs/10.1029/2021GL094364 doi: https://doi.org/10.1029/2021GL094364

Sorooshian, A., Anderson, B., Bauer, S. E., Braun, R. A., Cairns, B., Crosbie, E., ... Zuidema, P. (2019). Aerosol–cloud–meteorology interaction airborne field investigations: Using lessons learned from the u.s. west coast in the design of activate off the u.s. east coast. *Bulletin of the American Meteorological Society*, *100*(8), 1511 – 1528. Retrieved from https://journals.ametsoc.org/view/journals/bams/100/8/bams-d-18-0100.1.xml doi: 10.1175/BAMS-D-18-0100.1

Sorooshian, A., Corral, A. F., Braun, R. A., Cairns, B., Crosbie, E., Ferrare, R., ... Zuidema, P. (2020). Atmospheric research over the western north atlantic ocean region and north american east coast: A review of past work and challenges ahead. *Journal of Geophysical Research: Atmospheres*, *125*(6), e2019JD031626. Retrieved from https://agupubs.onlinelibrary.wiley.com/doi/abs/10.1029/2019JD031626 (e2019JD031626 2019JD031626) doi: https://doi.org/10.1029/2019JD031626

Stevens, B., Lenschow, D. H., Vali, G., Gerber, H., Bandy, A., Blomquist, B., ... van Zanten, M. C. (2003). Dynamics and chemistry of marine

stratocumulus—dycoms-ii. *Bulletin of the American Meteorological Society*, *84*(5), 579 - 594. Retrieved from https://journals.ametsoc.org/view/journals/bams/84/5/bams-84-5-579.xml doi: 10.1175/BAMS-84-5-579

Tomlin, J. M., Jankowski, K. A., Veghte, D. P., China, S., Wang, P., Fraund, M., ... Laskin, A. (2021). Impact of dry intrusion events on the composition and mixing state of particles during the winter aerosol and cloud experiment in the eastern north atlantic (ace-ena). *Atmospheric Chemistry and Physics*, *21*(24), 18123–18146. Retrieved from https://acp.copernicus.org/articles/21/18123/2021/ doi: 10.5194/acp-21-18123-2021

Tornow, F., Ackerman, A. S., & Fridlind, A. M. (2021). Preconditioning of overcast-to-broken cloud transitions by riming in marine cold air outbreaks. *Atmospheric Chemistry and Physics*, *21*(15), 12049–12067. Retrieved from https://acp.copernicus.org/articles/21/12049/2021/ doi: 10.5194/acp-21-12049-2021

Tselioudis, G., Rossow, W. B., Jakob, C., Remillard, J., Tropf, D., & Zhang, Y. (2021). Evaluation of clouds, radiation, and precipitation in cmip6 models using global weather states derived from isccp-h cloud property data. *Journal of Climate*, *34*(17), 7311 - 7324. Retrieved from https://journals.ametsoc.org/view/journals/clim/aop/JCLI-D-21-0076.1/JCLI-D-21-0076.1.xml doi: 10.1175/JCLI-D-21-0076.1

Twomey, S. (1974). Pollution and the planetary albedo. *Atmospheric Environment (1967)*, *8*(12), 1251-1256. Retrieved from https://www.sciencedirect.com/science/article/pii/0004698174900043 doi: https://doi.org/10.1016/0004-6981(74)90004-3

Wang, H., & Feingold, G. (2009). Modeling mesoscale cellular structures and drizzle in marine stratocumulus. part i: Impact of drizzle on the formation and evolution of open cells. *Journal of the Atmospheric Sciences*, *66*(11), 3237 - 3256. Retrieved from https://journals.ametsoc.org/view/journals/atsc/66/11/2009jas3022.1.xml doi: 10.1175/2009JAS3022.1

Wang, Y., Zheng, G., Jensen, M. P., Knopf, D. A., Laskin, A., Matthews, A. A., ... Wang, J. (2021). Vertical profiles of trace gas and aerosol properties over the eastern north atlantic: variations with season and synoptic condition. *Atmospheric Chemistry and Physics*, *21*(14), 11079–11098. Retrieved from https://acp.copernicus.org/articles/21/11079/2021/ doi: 10.5194/acp-21-11079-2021

Wood, R. (2006). Rate of loss of cloud droplets by coalescence in warm clouds. *Journal of Geophysical Research: Atmospheres*, *111*(D21). Retrieved from https://agupubs.onlinelibrary.wiley.com/doi/abs/10.1029/2006JD007553 doi: https://doi.org/10.1029/2006JD007553

Wood, R., Stemmler, J. D., Rémillard, J., & Jefferson, A. (2017). Low-ccn concentration air masses over the eastern north atlantic: Seasonality, meteorology, and drivers. *Journal of Geophysical Research: Atmospheres*, *122*(2), 1203-1223. Retrieved from https://agupubs.onlinelibrary.wiley.com/doi/abs/10.1002/2016JD025557 doi: 10.1002/2016JD025557

Yamaguchi, T., Feingold, G., & Kazil, J. (2017). Stratocumulus to cumulus transition by drizzle. *Journal of Advances in Modeling Earth Systems*, *9*(6), 2333-2349. Retrieved from https://agupubs.onlinelibrary.wiley.com/doi/full/10.1002/2017MS001104 doi: 10.1002/2017MS001104

Zheng, G., Sedlacek, A. J., Aiken, A. C., Feng, Y., Watson, T. B., Raveh-Rubin, S., ... Wang, J. (2020). Long-range transported north american wildfire aerosols observed in marine boundary layer of eastern north atlantic. *Environment International*, *139*, 105680. Retrieved from https://www.sciencedirect.com/science/article/pii/S0160412019326480 doi: https://doi.org/10.1016/j.envint.2020.105680

Zheng, G., Wang, Y., Wood, R., Jensen, M. P., Kuang, C., McCoy, I. L., ... Wang,

J. (2021). New particle formation in the remote marine boundary layer. *Nature Communications*, *12*(1), 527. Retrieved from `https://www.nature.com/articles/s41467-020-20773-1` doi: 10.1038/s41467-020-20773-1